Journal of Luminescence 236 (2021) 118113

Contents lists available at ScienceDirect

Journal of Luminescence

journal homepage: http://www.elsevier.com/locate/jlumin

Pedestal waveguides based on GeO_2-Bi_2O_3, GeO_2-PbO, Ta_2O_5 and SiO_xN_y cores as platforms for optical amplifiers and nonlinear optics applications: Review of recent advances

Julián H. Sierra [a], Daniel O. Carvalho [b], Luciana R.P. Kassab [c,*], Camila D. da Silva Bordon [a], Ricardo E. Samad [d], Niklaus U. Wetter [d], Marco I. Alayo [a]

[a] Escola Politécnica, Universidade de São Paulo (USP), 05508-010, São Paulo, Brazil
[b] Departamento de Engenharia Elétrica, Faculdade de Tecnologia (FT), Universidade de Brasília (UnB), 70910-900, Brasília, Brazil
[c] Faculdade de Tecnologia de São Paulo, CEETEPS, 01124-060, São Paulo, Brazil
[d] Instituto de Pesquisas Energéticas e Nucleares, IPEN-CNEN/SP, São Paulo, Brazil

ARTICLE INFO

Keywords:
Pedestal waveguides
Cr mask
Rare earth ions luminescence enhancement
Optical amplifiers
Gain enhancement due to Si nanoparticles
Integrated nonlinear optics

ABSTRACT

In this review we present recent advances regarding pedestal waveguides using different cores based on GeO_2-Bi_2O_3, GeO_2-PbO, Ta_2O_5 and SiO_xN_y materials for optical amplifiers and nonlinear optics applications. The pedestal platform, based on Si technology, is interesting for materials that are hardly etched by conventional techniques as is the case of heavy metal oxide cores. The present results review recent technological advances to fabricate pedestal waveguides with and without Cr mask. The fabrication mechanism that does not use Cr mask and avoids micromasking effect is shown. The advantages of this process are discussed as well as its appropriateness to produce pedestal waveguides for optical amplification at 1.53 μm and nonlinear optics applications. Comparison with pedestal waveguides prepared with Cr mask is also included to highlight the advantages that the new technique performed in the absence of Cr mask may provide, regarding propagation losses at the infrared region. Results of pedestal waveguides performance improvement, due to the scattering of large silicon nanostructures is also reviewed opening new possibilities for more efficient pedestal waveguides for optical amplification.

1. Introduction

Recent advances based on optical waveguides fabrication technology using the pedestal architecture are shown in the present work as well as possible future perspectives. The pedestal platform has demonstrated to be adequate mainly for materials that are highly inert to chemical etchants as it avoids the core etching [1–6]. Thus, it opens the possibility to fabricate waveguides with novel materials based on heavy metal oxide promoting the development of different integrated optical devices. In this context germanium and tellurium oxide glasses [7–11] exhibit adequate properties for photonics mainly due to their high refractive index when compared to silicates. Moreover, when doped with rare earth ions they exhibit interesting properties for optical amplifiers applications In particular GeO_2-PbO, GeO_2-Bi_2O_3, TeO_2–ZnO, TeO_2–WO_3–Bi_2O_3 proved to be adequate materials due to the following features: high refractive index (≥1.8), low melting temperatures (normally in the range 700–1200 °C), wide transmission window (visible to mid-infrared), and low cutoff phonon energy (500–800 cm^{-1}) [3,5,12,13]. We highlight that their reduced phonon energy increases the luminescence efficiency and reduces the low nonradiative losses favoring the frequency upconversion luminescence. They are also suitable for rare earth ions incorporation and show luminescence enhancement due to plasmonic effect of metallic nanoparticles as already reported in the literature [14–21]. Ultrafast response favored by metallic nanoparticles was also demonstrated and showed the potential of these materials for nonlinear optics applications [22–26].

Many platforms have been proposed for waveguides fabrication such as ribs, slabs and so on; in some of them, hollow core arrows are fabricated over self-aligned pedestals (SAP) [27,28]. On the other hand, for the pedestal platform reviewed in the present study, the core is deposited after the definition of the SiO_2 pedestal, using conventional photolithography and reactive ion etching technique. In this case, it is

* Corresponding author.
E-mail address: kassablm@osite.com.br (L.R.P. Kassab).

https://doi.org/10.1016/j.jlumin.2021.118113
Received 14 January 2021; Received in revised form 25 March 2021; Accepted 6 April 2021
Available online 16 April 2021

not necessary to etch the core material, which represents an advantage with respect to other techniques, mainly, for materials based on heavy metal oxide that are normally inert to chemical etchants [1–6]. Moreover, another advantage refers to the fact that there is no interaction between the light that propagates in the core and the etched sidewalls; consequently, lower propagation losses are reached when compared to other architectures as conventional rib [29–32] or strip waveguides [33,34].

Devices with applications in integrated nonlinear optics play an important role and have many applications. In particular, those optical devices based on materials with higher refractive index normally attend this requirement. The first platform used for integrated nonlinear optics was Silicon On Insulator (SOI) [35,36]. However, due to its narrow bandgap silicon material, which is used as core material for SOI optical devices, this platform does not represent a good alternative for nonlinear optics applications because of its high nonlinear losses. Moreover, there are other materials such as Silicon Nitride (Si_3N_4) and Hydex [37] that deserve attention, as they showed to be important potential candidates for parametric amplification, wavelength conversion and Frequency Comb Generation [38–43]. They are easily etched with conventional Reactive Ion Etching (RIE) techniques exhibiting low loss and presenting a larger operation bandwidth with respect to Si.

In addition to these materials, Tantalum Pentoxide (Ta_2O_5) can also be considered a very promising material for integrated nonlinear photonics applications [44–47]. Ta_2O_5 has a linear refractive index of n = 2.07, which is very close to that of silicon nitride. This optical property is important since it leads to waveguides with strong modal confinement and high nonlinear confinement (γ), without the burden of large nonlinear absorption that appears in materials like silicon, or other semiconductors. This large refractive index can also lead to more flexibility when executing dispersion engineering to optimize the efficiency of different parametric nonlinear phenomena and devices. This is the case when designing devices for parametric amplification, frequency comb generation and even wavelength conversion [38–43].

Due to the possibility of providing low propagation losses, the pedestal architecture appears as an interesting alternative for novel materials applications as optical amplifiers and nonlinear optics. In fact, materials that are difficult to etch tend to provide very high propagation losses since they tend to lead to larger scattering losses, associated with rougher surfaces, and other artifacts. Pedestal architecture facilitates the fabrication process and enables the production of longer lower loss waveguides when using such materials. Longer waveguides are important for nonlinear optics [48,49] due to the inherent cumulative nature of the nonlinear effects, as well as for waveguide optical amplifiers. If the losses are too high, the power within the waveguide falls within a few milimeters to a very small fraction of the power launched at its input making it impossible to obtain net gain in both types of devices [50,51].

Recently we reviewed [52] the use of the pedestal architecture prepared using a Cr mask and demonstrated the potential applications for optical amplification in the infrared region. In that report we discussed the advantages of pedestal architecture and showed some advances of the processes that lead to the optical waveguide's improvement. We reviewed the Mach-Zehnder interferometer structures that used TeO_2–WO_3–Bi_2O_3 core and showed the low propagation losses at 633 and 1050 nm as well as the possible applications for integrated optical sensors [2]. We also reviewed the fabrication of Yb^{3+}/Er^{3+} codoped TeO_2–WO_3–Bi_2O_3 pedestal waveguides and the possible applications as optical amplifiers operating at 1530 nm [3]. Moreover, we showed an improvement in the fabrication process of Yb^{3+}/Er^{3+} codoped GeO_2--PbO pedestal waveguides with gold nanoparticles that allowed gain enhancement of 50%, at 1530 nm [5]. In the mentioned review we investigated the influence of gold nanoparticles on Yb^{3+}/Tm^{3+} codoped GeO_2-PbO pedestal waveguide attributing the observed luminescence and gain enhancement to gold nanoparticles at 805 nm and showed that the metal dielectric composite based on GeO_2-PbO presents good prospects for applications in short distance optical network [53]. Regarding nonlinear optics we discussed the future perspectives of pedestal platform for integrated nonlinear optical device applications with respect to two characteristics: the possibility of exploring novel materials which could not be otherwise explored, for the reasons that we have mentioned above and second, the fact that the geometry of pedestal waveguides allows more degrees of freedom in dispersion engineering used for designing the waveguides. The last factor is particularly relevant, since besides the thickness and width of the core, which are also used to tailor the dispersion of rectangular strip waveguides, the height and width of the pedestal itself can be used in order to optimize dispersion for a particular application [54].

In the present review we intend to complement the previous mentioned works with more recent results and advances on the pedestal architecture using different routes for operation at 1.53 μm**.** We review some recent results of pedestal waveguides whose core was based on Yb^{3+}/Er^{3+} doped GeO_2-PbO with Si nanoparticles [55]; in this case the influence of Si nanoparticles is discussed as well as the improvement of the process for SiO_2 pedestal fabrication. Results of relative gain at 1.53 μm are shown and compared with those due to Si nanoparticles that are responsible for the elastic scattering that influences the effective optical path length and provides absorption cross-section increase with a positive impact on the optical properties and waveguide performance. Moreover, we present the results of a new technique developed to prepare the SiO_2 pedestal without Cr mask for Yb^{3+}/Er^{3+} doped GeO_2-PbO waveguides, that improved the optical performance and that was recently reported too [56]. A discussion and comparison with SiO_2 pedestal prepared with Cr mask is also included to highlight the advantages that the new technique without Cr mask provides, regarding the propagation losses. In both cases (process with and without Cr mask) the cores are prepared with the sputtering and plasma enhanced chemical vapor deposition (PECVD) techniques after SiO_2 pedestal fabrication which, as mentioned before, represents an interesting alternative for materials that are difficult to be etched. The experimental setup regarding the sputtering chamber with the different targets positioned in different holders is presented for all the cases, as well as the different parameters used during the deposition of the materials to produce the thin film of the waveguide core.

We also present a review of pedestal waveguides for nonlinear optics applications based on Ta_2O_5 and SiO_xN_y cores both prepared without Cr mask [57,58]. In these cases, the processes used for the core fabrication are discussed (sputtering and PECVD techniques). The experimental procedure to determine the nonlinear refractive index with pulse spectral broadening measurements based on self-phase modulation (SPM) is also reviewed. The nonlinear refractive index results are shown, as well as the possible applications for nonlinear optics. Finally, we present a discussion about the perspectives for the near future regarding both types of devices.

We start this review discussing results of optical gain in glasses based on GeO_2-PbO and GeO_2-Bi_2O_3 compositions (thin films and bulks). We briefly discuss these results materials as the present review deals with waveguides whose cores are fabricated with these materials; then we expose the reasons that lead pedestal waveguides based on thin films based of Ta_2O_5 and SiO_xN_y materials to be considered as suitable materials for nonlinear optics applications. We review the different procedures for pedestal waveguides fabrication, using Si technology, with and without Cr mask as well as the different methods for core deposition using the different materials (GeO_2-PbO and GeO_2-Bi_2O_3, Ta_2O_5 and SiO_xN_y). Finally, we review recent results using the pedestal architecture advances for optical amplification at 1.53 μm and for nonlinear optics applications and present perspectives for future too.

2. Glasses based on germanium oxide doped with rare earth ions: suitable materials for optical waveguides

In this section we briefly review some results of optical gain in glasses based on germanium oxides (thin films and bulks) that

demonstrate their appropriateness for optical waveguide applications. Relative gain enhancement of ~100% was demonstrated in the infrared region due to the presence of gold nanoparticles deposited on the top of cores produced with Yb^{3+}/Er^{3+} [5] and Yb^{3+}/Tm^{3+} doped GeO_2-PbO thin films [53]. Using a different method based on double waveguides amplifiers, written by femtosecond laser irradiation in Yb^{3+}/Er^{3+} doped GeO_2-PbO glasses (bulks), the potential of these materials for the fabrication of integrated optical amplifiers to operate at the third telecommunications window was shown [59]. The potential of bulk materials for optical amplification without waveguides inside was also reported. Using a simple method that does not require the complex ones for waveguide fabrication, it was demonstrated the influence of Al_2O_3 on optical gain performance in Nd^{3+} doped GeO_2-PbO glasses and the resulting improvement at 1064 nm [13]; moreover the addition of Al_2O_3 allowed relative gain increase of more than 100% and demonstrated an alternative to improve the performance of lasers and amplifiers without the use of metallic nanoparticles. By similar procedure it was demonstrated that Tm^{3+} doped GeO_2–Bi_2O_3 glasses with silver nanoparticles have potential applications for devices that require optical gain and intense photoluminescence at 1470 nm [12]. In this case, the local field enhancement attributed to silver nanoparticles provided a large enhancement (~500%) of the relative gain at 1470 nm.

3. Thin films based on Ta_2O_5 and SiO_xN_y materials: suitable materials for nonlinear optics applications

Previously, pedestal waveguides were not used for nonlinear optical applications. Only in the last couple of years, waveguides fabricated with two different materials using this platform have been demonstrated: Ta_2O_5 [57] and SiO_xN_y [58]. Tantalum oxide is well known as an excellent optical material, which for decades has been used as anti-reflective coating for different applications due to its high refractive index and high transparency [60–62].On the other hand, silicon oxynitride is a very versatile material, since its refractive index can be tuned varying the deposition parameter by means of the PECVD technique: from the refractive index of silicon dioxide (n = 1.46) to that of silicon nitride (n = 2.0) [63–68].

The advantage of using the pedestal architecture for the fabrication of Ta_2O_5 waveguides has to do with the difficulty in determining a dry etch recipe for defining the sidewalls of this material by photolithography in conjunction with direct etching of the material itself. Although tantalum oxide has all the advantages mentioned in the previous sessions as a nonlinear material, defining appropriate parameters for etching, regarding plasma chemistry, chamber pressure, gas flow rates, etc, is not an easy task, particularly when the set of gases available is limited. In fact, when attempting to fabricate strip waveguides by directly etching this material with CHF_3 and SF_6 gases available in our facility, the resulting waveguides did not even guide light. In this case, light was attenuated in such a short distance, and it was not even possible to measure propagation losses. The reason for the prohibitively high attenuation has to do with the large sidewall roughness which resulted from the Reactive Ion Etching (RIE) of these waveguides. This effect has been observed consistently when metal hard mask is used or when etching materials with metals in their composition are etched using capacitively coupled RIE etching in conjunction with fluorinated gases. This effect is related with sputtering and re-deposition of the metallic element, such as chromium or tantalum, over the surface of the sample. Since metallic elements tend to be more inert to the plasma chemistry, they form clusters which produce a micro-masking effect. As a result, the surface of the sample tends to become rougher and pillar shaped structures, often referred to as 'micro-grass', are formed on the surface of the sample. All these artifacts cause excessive scattering of light and increase the propagation losses [6]. This is where the advantage of using pedestal becomes evident, since it makes it possible to utilize materials that otherwise could not be used to define waveguides.

As for silicon nitride, we have demonstrated in previous works that pedestal waveguides presented superior characteristics in comparison with other processes, as for instance, rib waveguides with Si_3N_4 as core (i.e., the propagation losses were half those measured with rib waveguides) [1–6].

4. Pedestal waveguides different fabrication processes using Si technology: with and without Cr mask

This section presents two different mechanisms used for the pedestal architecture fabrication, one of them using Cr mask and the other a different procedure that does not make use of Cr mask.

For the case of the pedestal waveguide (Yb^{3+}/Er^{3+} doped GeO_2–Bi_2O_3) produced with Cr mask the following steps were used: cleaning of the silicon substrate, SiO_2 cladding layer deposition, chromium film deposition followed by the deposition and mask definition of the photoresist. Then after the chromium mask definition the etching of the SiO_2 was performed, followed by the chromium removal. The final step is the core deposition using the sputtering technique, which is an advantage, as mentioned before, as it provides the deposition of different materials [5,6,53]. The performance enhancement of the pedestal waveguides demonstrated in our previous report were due to advances included in the following fabrication process of the pedestal waveguide; enhancement of the steps used for the SiO_2 etching (RF power of 100 W and gas flow rate of 40 sccm for both CHF_3 and O_2, under a chamber pressure of 50 mTorr) to promote better pedestal definition and reduction of the Cr mask layer thickness in 70% to decreasing the amount of chromium residues after its removal and attenuating the micromasking effect [69]. Normally residues from the incomplete removal of the Cr mask layer contribute to the columnar growth (pillar structures adjacent to the lateral surface of the waveguides) whose proximity to the optical field confined in the core layer compromises the light guiding due to growth of propagation losses. Fig. 1 shows scanning electron microscopy (SEM) images that illustrates an example of pillar structures due to the micromasking effect. Another change that deserves attention was the core layer thickness reduction from 1000 to 400 nm as well as the pedestal height increase that originates a larger distance between the pillars structures of chromium residues and the core waveguide. For the Yb^{3+}/Er^{3+} doped GeO_2 –Bi_2O_3 waveguide reviewed in the present study, the pedestal height was of 1.2

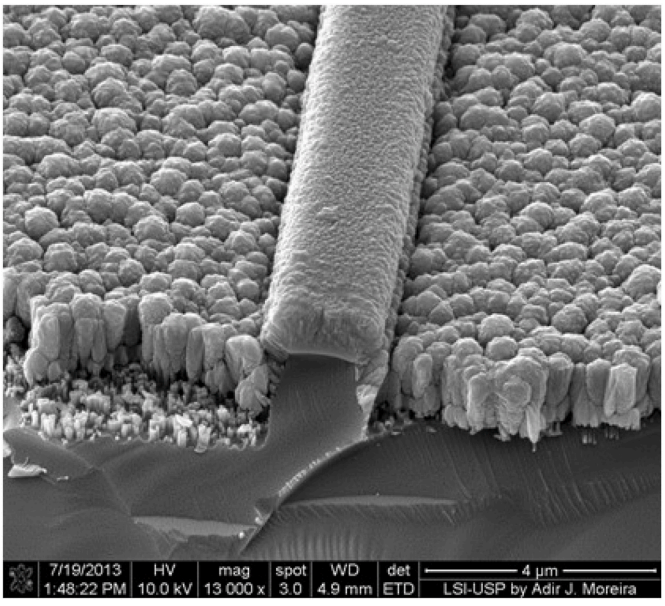

Fig. 1. SEM image of a pedestal waveguide prepared with Cr mask and the pillar structures adjacent to the lateral surface of the waveguides due to micromasking effect.

μm.

Regarding the waveguide produced without Cr mask, we developed a different procedure that was used for the Yb^{3+}/Er^{3+} doped PbO-GeO_2, Ta_2O_5 and SiO_xN_y [56–58] waveguides in which a photoresist was used to define the waveguide lateral dimensions by wet etching of a thin thermal oxide, which was then used as a mask for the silicon pedestal etched with reactive ion etching. This process results in smoother pedestal surfaces, reduces scattering losses, and also avoids micro-masking by the re-deposited chromium. The following steps are used in this process: growth of a 150 nm-thick thermal silicon dioxide film, spin-coating of the wafer with photoresist, followed by photolithography and etching of the thin thermal silica layer in BOE (*Buffered Oxide Etch)*; finally, to form the pedestal, the RIE etching of the silicon substrate was performed followed by the removal of the photoresist and wet oxidation of the silicon substrate. The last step was the deposition of the material to produce the core using the sputtering or PECVD techniques which is presented in the next section. Figs. 2 and 3 show the processes of the pedestal fabrication with and without Cr mask, respectively.

5. The processes for the core deposition

The core deposition processes used for the Yb^{3+}/Er^{3+} doped PbO-GeO_2 (PGO) [56] and Yb^{3+}/Er^{3+} doped GeO_2–Bi_2O_3 (BGO) [55] waveguides were similar and will be explained in this section. In both cases, the RF magnetron sputtering technique was used. During the deposition of the PGO waveguide, Er_2O_3 pellets (1 cm diameter) and Yb_2O_3 commercial target (5 cm diameter) were placed on the same holder in the sputtering chamber using 20 W RF power, whereas the PbO-GeO_2 target (in wt%: 60PbO-40GeO_2 and 5 cm diameter) was placed in a different one with 60 W RF power. The sputtering chamber operated with Argon gas (18 sccm flow) at 5 mTorr pressure and distance of 15 cm between the targets and the substrate. After 6 h of deposition, the PGO waveguide, with 410 nm pedestal height was annealed at 400 °C for 10 h; this procedure is important to provide the incorporation of rare earth ions in the trivalent form as well as to enhance the transparency of the thin film. Fig. 4 show scanning electron microscopy (SEM) image of PGO waveguide in which we notice the lack of pillar structures mentioned before (Fig. 1) due to the advances included in the new fabrication process explained in the section before. PGO waveguides with gold were fabricated as follows: a thin gold layer was deposited over the PGO waveguide using a commercial gold target (99.99% purity), sputtered during 5 min, Argon gas at 5 mTorr pressure and 5 W RF power. Moreover, a shutter with holes was placed between the gold target and the PGO waveguide to reduce the deposition rate of gold [53–56]. The correct gold concentration deserves attention as high concentration, that normally promotes ohmic dissipation [70], has to be

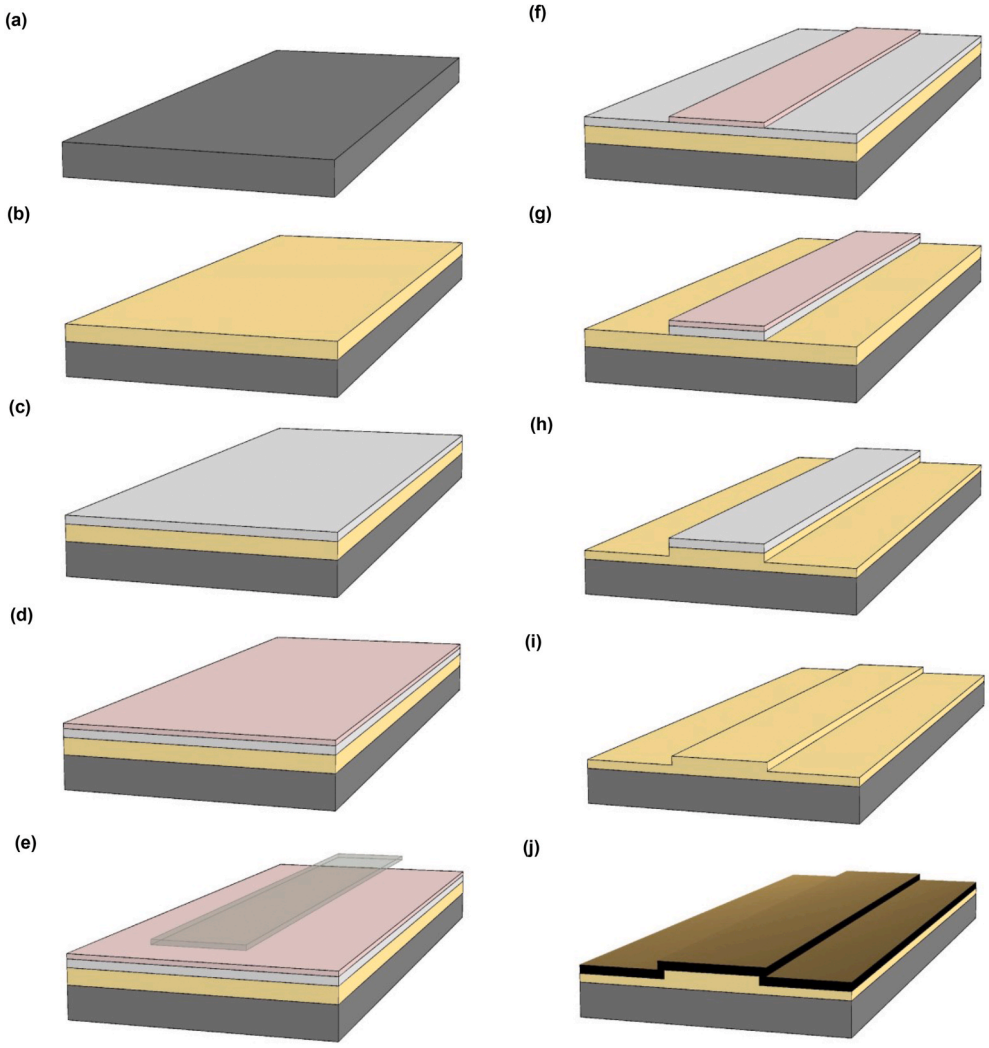

Fig. 2. Schematic diagram of the pedestal optical waveguide fabrication process using Cr maks: (a) standard cleaning of the silicon substrate; (b) SiO_2 cladding layer deposition; (c) chromium film deposition; (d) photoresist deposition; (e) development of the photoresist; (f) photoresist mask definition; (g) chromium mask definition; (h) etching of the SiO_2; (i) chromium removal and; (j) core deposition [5].

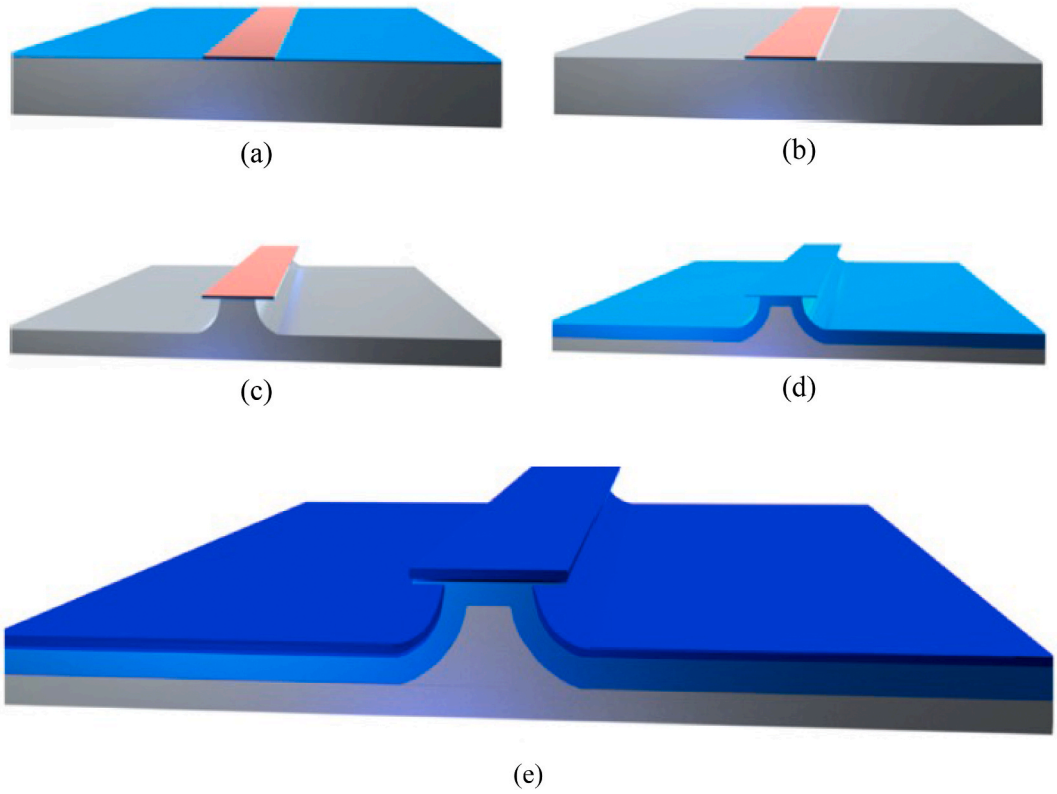

Fig. 3. Pedestal waveguide fabrication process: (a) growth of a 150 nm-thick thermal silicon dioxide film on a silicon wafer, spin-coating of the wafer with photoresist and photo-lithography; (b) wet etching of the SiO2 layer in BOE (Buffered Oxide Etch); (c) RIE etching of the silicon substrate to form the pedestal; (d) removal of the photoresist and wet oxidation of the silicon substrate and; (e) core deposition [56].

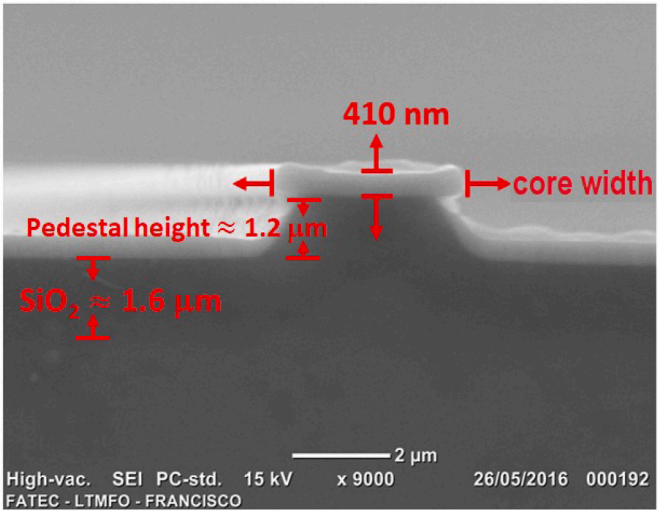

Fig. 4. SEM image of PGO pedestal waveguide produced without Cr mask [56].

avoided, therefore, a short period deposition was used (5 min). The waveguide was then annealed at 400 °C during 1 h to nucleate gold nanoparticles following procedure already consolidated for nucleation of metallic nanoparticles [8,29,53].

A similar procedure was used for BGO waveguide fabrication [55]. However, in this case pellets of Er_2O_3 and Yb_2O_3 and GeO_2-Bi_2O_3 target (in wt%: 58.4GeO_2-41.6Bi_2O_3) were placed on the same holder, operating at 70 W RF power, and sputtered simultaneously with the commercial Si target, placed on another holder, at 9 W RF power. As in the case of the gold deposition, a shutter with holes was placed between the Si target and the BGO waveguide to reduce the deposition rate of Si. Annealing at 440 °C during 3 h was performed to nucleate Si nanoparticles. Fig. 5 shows a SEM image of BGO waveguide, fabricated using the process shown in Fig. 2. Fig. 6 illustrates the targets, pellets and the shutter with holes used for the BGO waveguide core deposition.

Reactive DC (1.77 kV) sputtering technique was used in the case of the Ta_2O_5 pedestal waveguide [57]. During the deposition of the Ta_2O_5 waveguide, a tantalum commercial target (99.9% of purity) was used with a gaseous mixture of O_2 and Argon gas at 1.4 mTorr total pressure and distance of 15 cm between the target and the substrate. A rotating chuck inside the deposition chamber was used to improve uniformity over the pedestal samples. In this case, a core thickness of 430 nm was obtained for a total deposition time of 50 min. Moreover, the pedestal

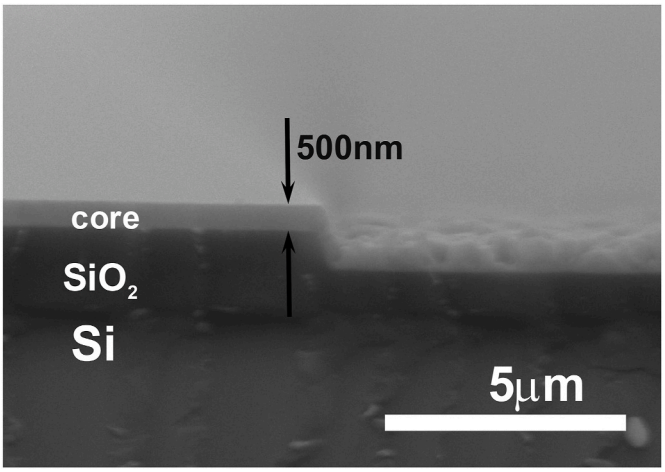

Fig. 5. SEM image of BGO pedestal waveguide produced with Cr mask [55].

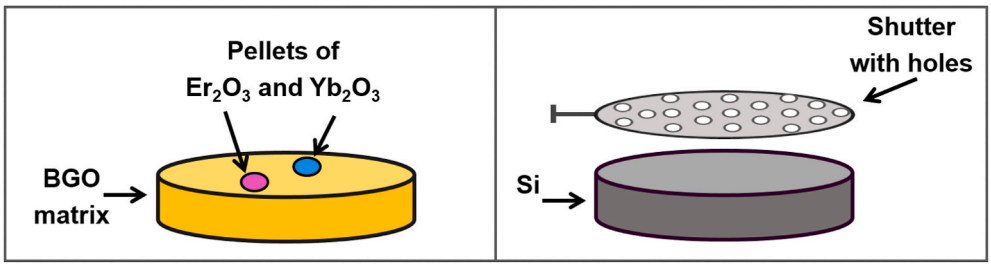

Fig. 6. The targets, pellets and the shutter with holes used for the BGO waveguide core deposition.

height in this case was 3.7 μm and the process illustrated in Fig. 3 (without Cr masking) was utilized to fabricate these waveguides.

Regarding SiO_xN_y pedestal waveguide deposition, PECVD technique was used with 200 W of RF power for a substrate holder with 20 × 20 cm^2 of area [58]. The gases used in the PECVD deposition were nitrous oxide (N_2O) with 27.2 sccm flow, nitrogen (N_2), with 47.8 sccm flow and silane (SiH_4) with 30 sccm flow [58]. Pressure and deposition temperature were set to 33 mTorr and 320 °C, respectively [58], for 90 min, to obtain the SiO_xN_y film with 1470 nm thickness. The pedestal height in this case was 3.7 μm and the process illustrated in Fig. 3 was utilized to fabricate these waveguides as well.

6. Pedestal waveguides based on metal dielectric composites: different routes for operation at 1.53 μm

There is a lack of information in the literature with respect to the scattering properties of Si nanocrystals and their influence on the optical amplification [55]. For this reason, we review some optical results regarding the performance improvement of BGO pedestal waveguides due to scattering by large silicon nanostructures that showed that appropriate disorder may open an avenue for design and manufacture of novel photonic devices.

In this investigation the following points were highlighted: the addition of relatively large Si nanoparticles (25–30 nm diameter) enhances the effective optical path length (Fig. 7), and consequently, the effective absorption cross-section at 980 nm and luminescence growth [55]; moreover, the presence of a high concentration of Si nanostructures (high refractive index ~3.7) improves the waveguide performance as the average effective index of the core is increased. The photoluminescence enhancement at 520 nm and 1530 nm can be seen in Fig. 8a and 8 b, respectively. A relative gain increase of 50% is measured

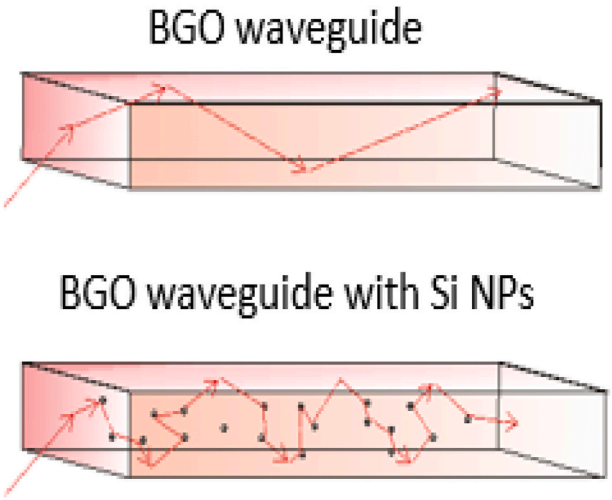

Fig. 7. A schematic view of the increase of optical path-length in a waveguide with Si nanostructures (scatterers) in comparison with the one without Si nanostructures [55].

at 1542 nm (10 mm sample length) and presented in Fig. 9a and 9 b. All these results are attributed to the elastic scattering provided by the Si nanostructures that influences the effective optical path length and provides absorption cross-section growth. The present investigation can be extended to different hosts and open new possibilities for more efficient waveguides produced with the pedestal architecture using Si nanostructures.

Regarding the PGO pedestal waveguide we review some results that show the performance improvement obtained in the absence of the Cr mask [56]. Fig. 10 compares the propagation losses results (at 1068 nm) obtained using the top view technique [71] for the pedestal waveguide studied in the present review with the one prepared with chromium mask: in both cases a decrease takes place with increasing waveguide width. For the PGO waveguide propagation losses of 1 dB/cm are observed for 80 μm waveguide width, whereas for those smaller than 4 μm, an abrupt increase occurs. The near field profile of the PGO waveguides can be seen in Fig. 11 where we observe that larger waveguides exhibit multimode behavior and the smaller ones, single mode behavior. We highlight that the propagation losses are significantly smaller than those found for pedestal waveguides fabricated using chromium mask.

Fig. 12 a presents the relative gain (signal enhancement) as a function of the excitation power for PGO pedestal waveguides with and without gold nanoparticles (at 1.53 μm). The maximum relative gain observed for 6 μm width is enhanced in 180% in the presence of gold nanoparticles, deposited on the waveguide. This signal growth is due to the local field intensity increase in the vicinity of the nanoparticles, that enhance the rare earth excitation density. Fig. 12 b shows transmission electron microscopy results of gold nanoparticles with average size around 4 nm; inset shows the electron diffraction pattern that corroborates the presence of gold crystalline nanoparticles (face centered cubic).

Another point that deserves attention is the possibility to obtain light guiding for waveguides with 6 μm width. This was not possible in previous works based on PGO waveguides prepared with Cr mask [5].

Is it also important to add that the fabrication of heavy-metal based waveguides was benefited by the pedestal architecture since there is no need to etch the core, a procedure that normally depends on the host chemical composition. This fact represents an advantage when compared to the technique used in the production for instance of rib waveguides [29] and simplifies the optical waveguide fabrication process.

The routes for the pedestal waveguides fabrication, based on Si technology reviewed in the present work allows optical amplifier performance optimization, can be extended to different metal dielectric composites and opens the possibility to fabricate different photonic devices. Table 1 summarizes some results obtained in different waveguides for operation at the infrared region.

7. Pedestal waveguides for nonlinear optics applications: a review of recent advances for Ta_2O_5 and SiO_xN_y core layers

In this section we review pedestal waveguides using Ta_2O_5 [57] and SiO_xN_y [58] cores, aiming at integrated nonlinear optics applications.

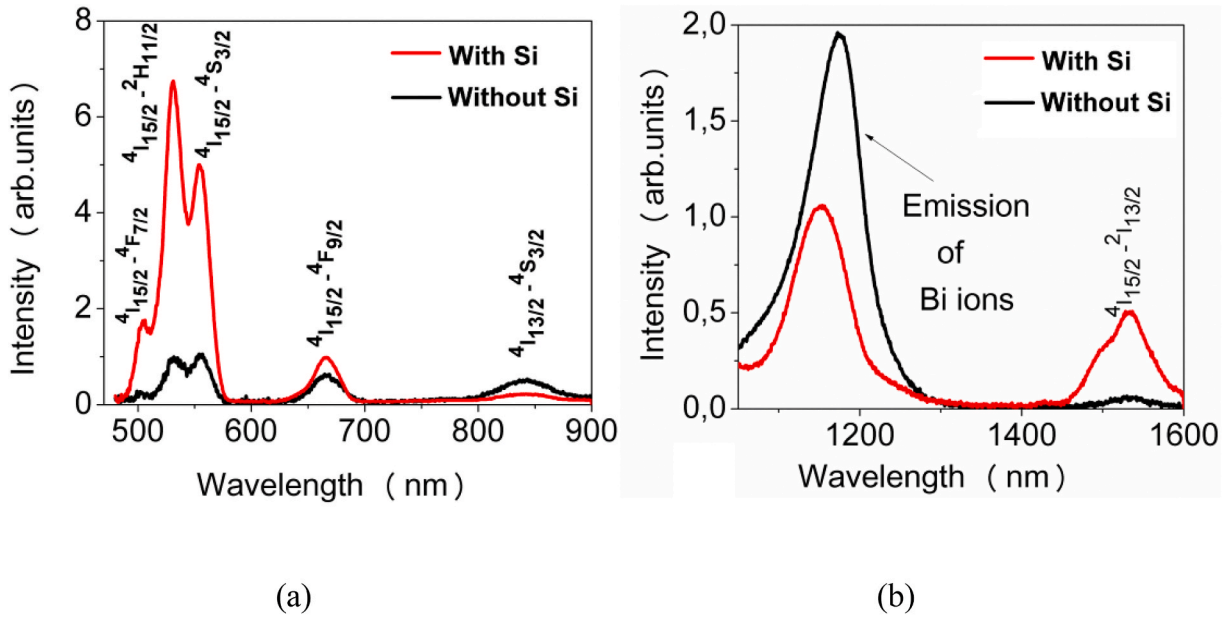

Fig. 8. Photoluminescence spectra of BGO thin films, with and without Si, under excitation at 980 nm in (a) the visible and (b) the near infrared region [55].

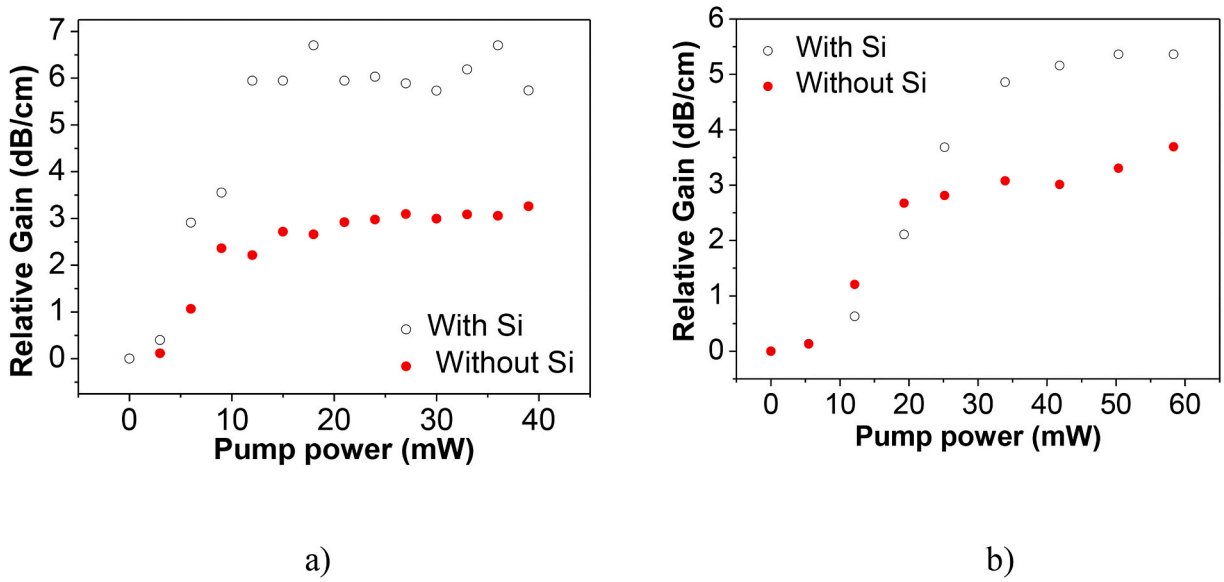

Fig. 9. Relative gain of BGO waveguide (at ~1.53 μm) as a function of the pump power at (a) a fixed position of 2 mm measured from the top of the waveguide and (b) measured at the exit facet (10 mm).

Using pedestal waveguides fabricated with these materials, high nonlinear refractive indices can be obtained leading to strong self-phase modulation. Due to the pedestal structures, these waveguides also present low propagation losses as will be shown.

Fig. 13 a presents SEM image of a Ta_2O_5 waveguide with pedestal of 3.6 μm height and core layer of 430 nm height and 5 μm width. In this figure, we notice a large separation between the core and the silicon layer as well as the Ta_2O_5 slab waveguides formed on both sides of the pedestal. The fabrication process illustrated in Fig. 3 leads to the appearance of a 'hat' shaped structure. This geometry avoids any Ta_2O_5 deposition immediately underneath the lateral 'hat'. All these characteristics are relevant to provide low leakage losses. Due to the high refractive index contrast, the mode is mainly confined in the core, as is shown in Fig. 13 b, that shows the fundamental mode obtained via a Finite Element Method (FEM) mode analysis, which was performed for the geometry of the fabricated waveguides. The losses were measure using the top view technique and the results are in Fig. 14. Low propagations values can be seen: 1.6 dB/cm for narrower waveguides, whereas of 0.1 dB/cm for the larger ones.

These small losses are attributed to the modified pedestal process presented in Fig. 3 [56], which does not make use of a Cr mask. Moreover, no micromasking induced pillar structures were observed in the neighborhood of the waveguide lateral surface. This is also attributed to the absence of the Cr mask during the pedestal fabrication process. Another point that deserves attention is that the propagation losses are significantly smaller than those presented in previous studies of Ta_2O_5 strip waveguides, in which conventional processes were used and typical propagation losses were of 2.4 dB/cm [72]. In fact, the present results reinforce the fact that the route for pedestal waveguides fabrication reviewed in this work represents a good alternative for reducing losses.

The nonlinear refractive index of the core material is 5.8×10^{-19} m^2/W, measured with ultrashort pulses at 785 nm for waveguides with

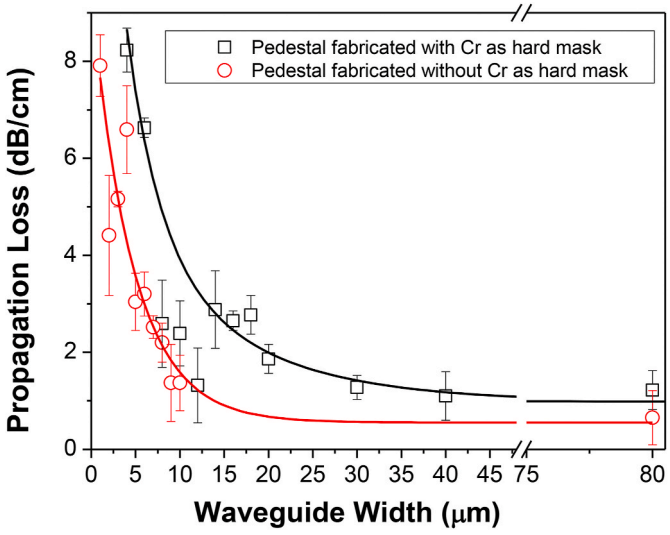

Fig. 10. Propagation losses of PGO waveguides prepared with and without Cr mask (1068 nm). The data from the waveguide fabricated without Cr mask was obtained from Ref. [56].

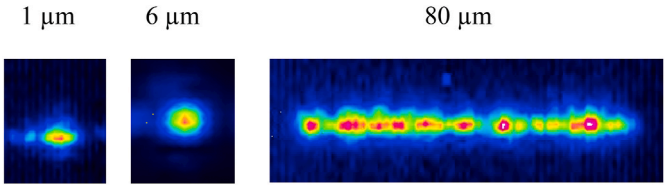

Fig. 11. Near field profile of PGO waveguides for different widths at 1068 nm.

widths ranging from 7 μm to 100 μm, using the non-linear optical phenomena of self-phase modulation (SPM). This value is more than one order of magnitude larger than that of silica [73]. Fig. 15 illustrates the experimental setup used for the self-phase modulation technique [58].

Ultrashort pulses lasting 23 fs (FWHM) generated by a Ti:sapphire amplified laser system (Femtopower Compact Pro HR/HP) centered at 785 nm, with 40 nm of bandwidth (FWHM), in a 4 kHz repetition rate train of pulses were coupled to the waveguides using a 10x microscope objective. A half-wave plate and polarizer were used to control the power and set the polarization of the pulses entering the waveguide. As the power was increased, spectra of the pulses exiting the waveguide, which were measured using an Optical Spectrum Analyzer (OSA), became wider due to the SPM. The amount of spectral broadening can be directly correlated with the nonlinear index of the medium in which light propagates, which in this case was the core of the pedestal waveguide. The results of the measured pulse spectra for different values of peak power at the waveguide injection are in Fig. 16, where we notice that the pulse spectral width increases from 44 nm ($P_0 = 790$ W) to 76 nm ($P_0 = 1.7$ kW). Hence, the present results indicate that pedestal

Table 1
Summary of pedestal and rib waveguides with different materials.

Waveguide type (width)	Material	Gain (dB/cm)	Losses (dB/cm)
Pedestal (18 μm)	Yb^{3+}/Er^{3+} codoped TeO_2–WO_3–Bi_2O_3 [3,52]	3.7	2.5 (1050 nm)
Rib (1.5–3 μm)	Er^{3+} codoped TeO_2 [74]	3.0	~0.4 (1100–1500 nm)
Pedestal (70 μm)	Er^{3+}/Yb^{3+} codoped PbO–GeO_2 (GP-B) [6,52]	6.0 3.5	1.0 (1068 nm) 2.0 (1068 nm)
(12 μm)			
Rib (4 μm)	Er^{3+}/Yb^{3+} codoped PbO–GeO_2 with gold nanoparticles [29,52]	4.3	2.0 (1050 nm)
Pedestal (30 μm)	Tm^{3+}/Yb^{3+} codoped PbO-GeO_2 with gold nanoparticles (10 min) [52,53]	22.0	5.0 (1068 nm)
Pedestal (100 μm)	Er^{3+}/Yb^{3+} codoped GeO_2 –Bi_2O_3 with Si nanoparticles [55]	5.5	Not available
Pedestal[a] (6 μm)	Er^{3+}/Yb^{3+} codoped PbO–GeO_2 with gold nanoparticles [56]	7.8	2.5 (1068 nm)

[a] Prepared without Cr mask. In this device it was obtained propagation losses below 1 dB/cm for waveguides widths larger than 20 μm.

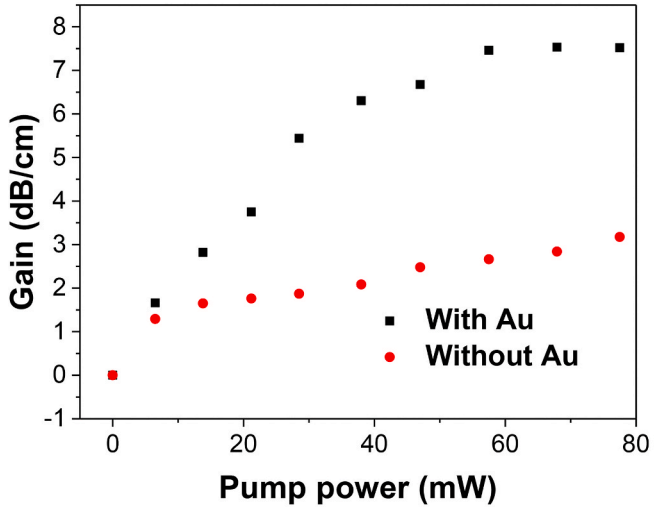

(a)

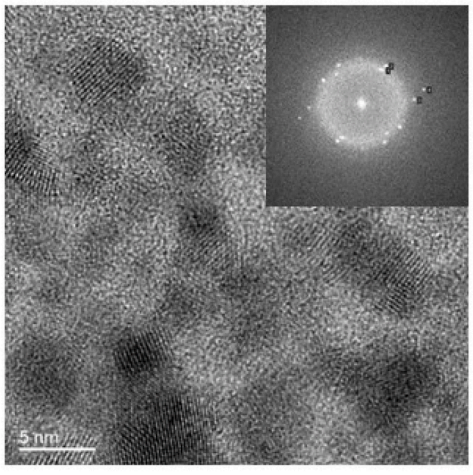

(b)

Fig. 12. (a) Relative gain at 1.53 μm (980 nm excitation) as function of the pump power of PGO pedestal waveguide, with and without gold nanoparticles (4 μm width and 1 cm length) and, (b) Transmission electron microscopy results of gold nanoparticles with average size around 4 nm (inset shows the electron diffraction image) [56].

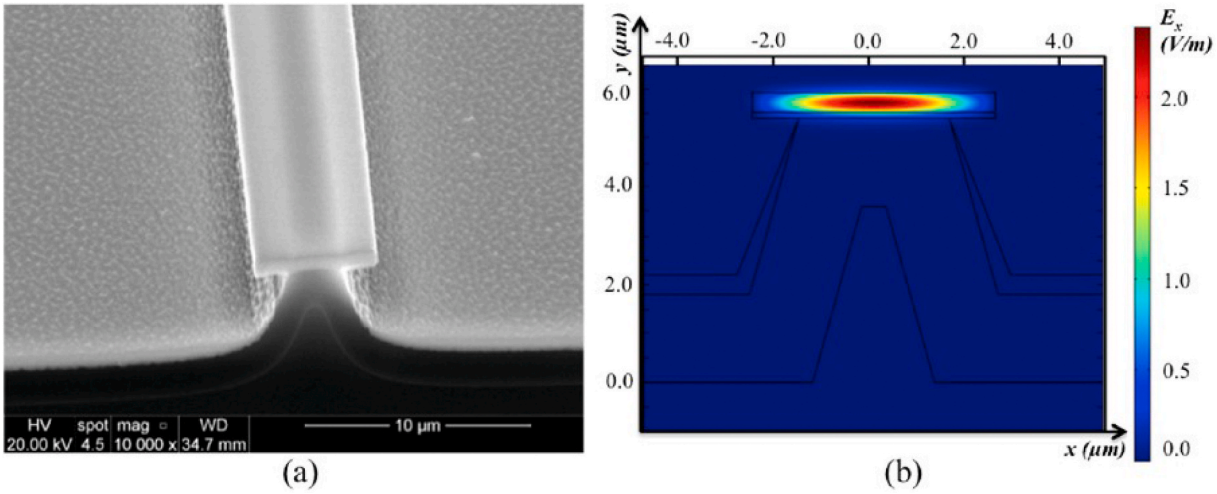

Fig. 13. (a) SEM image of Ta_2O_5 pedestal waveguide with 5 μm width (b) Magnitude of the electric field component associated with the fundamental mode waveguide, obtained by FEM mode analysis [57].

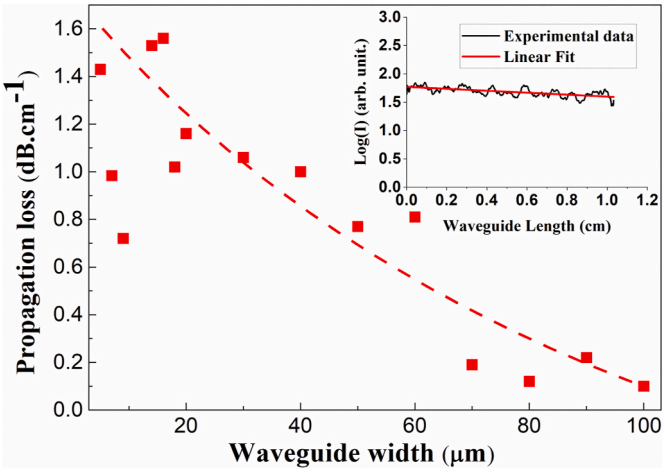

Fig. 14. Propagation loss results of Ta_2O_5 pedestal waveguides in the 5–100 μm width range. The inset shows the slope of the measured light intensity captured by the CCD camera as function of the optical waveguide length [57].

waveguide is promising for several applications such as supercontinuum generation, wavelength conversion and parametric amplification. The results reviewed in this section demonstrate that T_2O_5 oxide pedestal platform is a strong potential candidate for integrated nonlinear optics devices.

Here we would also like to review another alternative for nonlinear

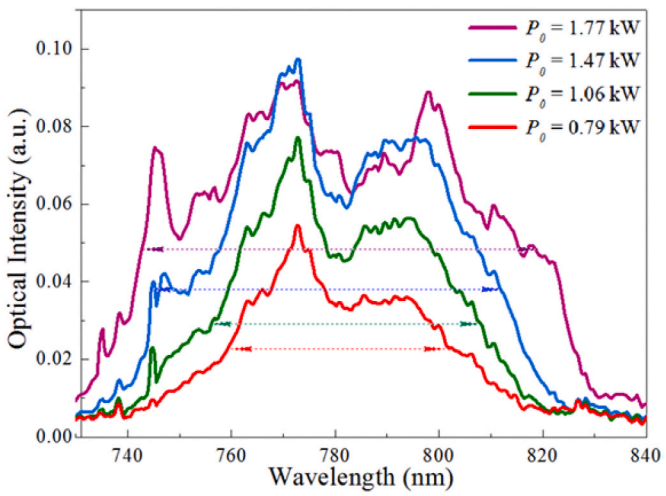

Fig. 16. Intensity spectra at the output of Ta_2O_5 waveguides for different peak powers [57].

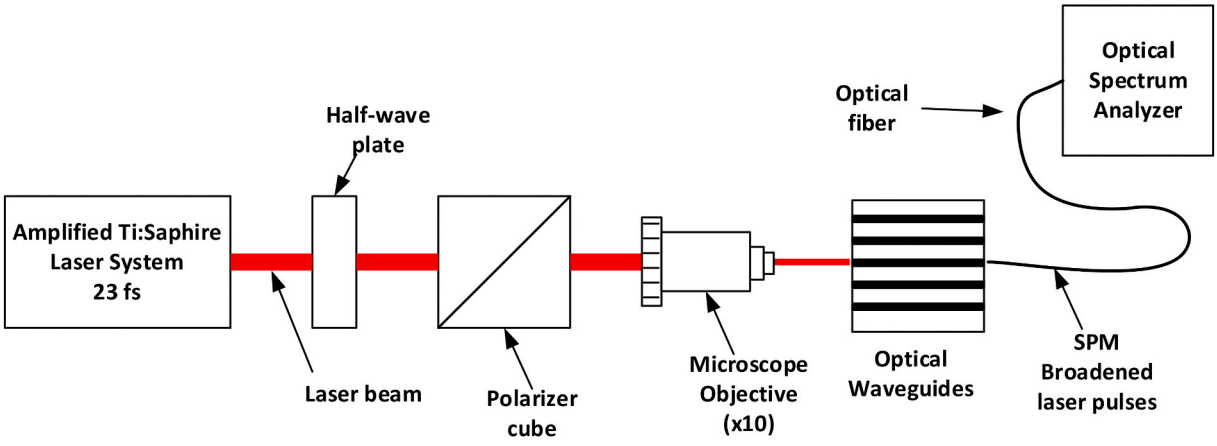

Fig. 15. Experimental setup used for self-phase modulation technique [58].

optics applications based on silicon oxynitride (SiO_xN_y) [58] pedestal waveguides fabricated as explained in sections 4 and 5. SEM images of the pedestal waveguide can be seen in Fig. 17a and 17 b, before and after the deposition of the SiO_xN_y core. Low roughness can be observed as well as the integrity of the pedestal after the core deposition. Losses of 1.63 dB/cm were measured using the top view technique, that was also employed in the other cases as it preserves the device integrity, unlike the cut back method. To determine the nonlinear refractive index, pulse spectral broadening measurements based on self-phase modulation (SPM) were used as well. In this case, the same experimental setup as described for the Ta_2O_5 (Fig. 15) was also used. The result of the measurements showed that the nonlinear refractive index of the SiO_xN_y core layer is 2.11×10^{-19} m^2/W which indicates that this material can be used for important nonlinear optical applications, such as photonic crystal fibers, optical converters and amplifiers, among others. Table 2 summarizes the present results with those that uses strip platform with Ta_2O_5 as core [74]. We observe that pedestal platform provides better performance as the nonlinear parameter is enhanced by more than 100%. Moreover, the propagation losses are also significantly smaller with respect to those of strip platform.

Table 2
Summary of pedestal, strip and bulk waveguides used for accessing the nonlinear index of different materials.

Waveguide type	Material	n_2 ($x10^{-19}$ m^2/W)	Losses (dB/cm)
Pedestal[a]	Ta_2O_5 [57]	5.80	0.1 (633 nm)
Pedestal[a]	SiO_xN_y [58]	2.11	~1.63 (633 nm)
Strip	Ta_2O_5 [72]	21.4	2.4 (800 nm)
Strip	Silicon enriched nitride [75]	14.0	~1.0 (1550 nm)
Bulk	Ta_2O_5 [76]	2.57	not available

[a] Prepared without Cr mask.

8. Perspectives for the near future

The recent progress achieved with pedestal waveguides for both applications, optical amplifiers and nonlinear optical (NLO) devices indicate that in the near future, more complex devices will be possible using a variety of novel materials regarding this platform. With respect to NLO, the demonstration of low loss and high nonlinear index using tantalum oxide and silicon oxynitride, it is very likely that devices such as ring resonators with very high quality factors are going to be designed using these materials. Efforts should also be made towards optimizing the optimum dispersion for applications such as Frequency Comb Generation and Parametric amplification. All of these will culminate in devices with outstanding characteristics in terms of amplification gain and frequency conversion efficiency. Moreover, the results of optical amplifiers presented in this review indicate the possibility to fabricate other pedestal waveguides to operate at different wavelengths. Different rare earth ions used as doping will allow applications in different regions of the electromagnetic spectrum. The addition of metallic nanoparticles represents an alternative to optimize the waveguides performance, as exposed in the present review. Besides the pedestal platform shown produced in the absence of Cr mask can be extended to different hosts regarding other integrated photonic devices. For larger waveguides width only the higher order modes that do not transport a large fraction of the energy and have a lower confinement factor, interact strongly with the waveguide sidewall roughness resulting in lower propagation losses above 20 μm waveguide width. The lower the waveguide width, the higher will be the propagation loss, once all guided mode, including the lowest order ones, interact with the waveguides sidewall roughness and then couple into different modes. Then light scattering due to surface imperfections is the main source of losses. Efforts should be done in the future to reduce the propagation losses, mainly regarding smaller waveguides width that exhibit single mode behavior; this limitation has to be overcome by improving the Si pedestal waveguide fabrication without Cr mask, as for example, the type and thickness of the photoresist used as photolithographic mask in the definition of the pedestal lateral dimensions by RIE technique. Procedures used for removal of the photoresist and wet oxidation of the silicon substrate can also be optimized.

9. Conclusion

We have reviewed the recent advances in optical amplifiers and nonlinear optics devices using pedestal platform. A novel pedestal fabrication procedure has made it possible to measure the nonlinear refractive index of SiO_xN_y and Ta_2O_5, leading to n_2 values of 2.11×10^{-19} m^2/W and 5.8×10^{-19} m^2/W, respectively. By using these materials, it was possible to obtain lower losses than those with alternative

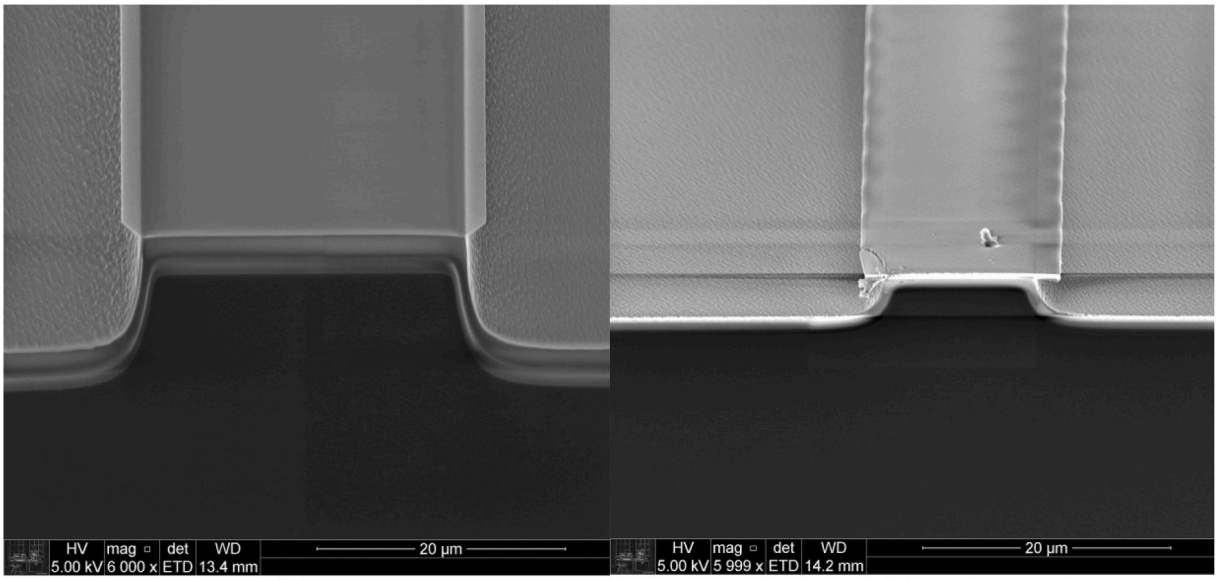

Fig. 17. SEM images of the pedestal structure a) before and b) after the deposition of the core layer [58].

platforms. This lays the groundwork for the exploration of other materials as well as for the development of different nonlinear optics devices, such as parametric amplifiers, and wavelength converters. The same applies to optical amplifiers whose procedures reviewed in the present work can be extended to other hosts regarding integrated photonic devices for operation in different wavelengths of the electromagnetic spectrum. Two different routes were reviewed regarding operation at 1.53 μm. One of them did not use Cr mask for the pedestal fabrication and consequently avoided micromasking effect leading to lower propagation losses. In this case gold nanoparticles deposited by sputtering over the core waveguide led to relative gain growth by 180% that reached 7.8 dB/cm in waveguide width of 6 μm. We highlight that it was not possible to measure the gain for rare earth ions doped PbO-GeO_2 pedestal waveguides prepared with Cr mask in core widths smaller than 12 μm (gain of 3.5 dB/cm, as shown in Table 1). This fact represents another advantage for the construction of waveguide amplifiers based on the pedestal architecture produced without the Cr mask.

The other route based on the use of Cr mask took into account the addition of relatively large Si nanoparticles (25–30 nm diameter) that provided effective optical path length increase and consequently, the effective absorption cross-section enhancement at 980 nm. Then luminescence growth took place as well as the relative gain increase of 50%, at 1542 nm, attributed to the elastic scattering provided by the Si nanostructures that influenced the effective optical path length. The strategy of introducing disorder by appropriate amount of Si nanostructures opens new possibilities for pedestal waveguides fabrication and expands their applications in photonics.

In both routes, as the material used as core layer does not need etching procedures, the fabrication process is simplified with respect to other platforms. So, the technology based on pedestal architecture raises the possibility to explore novel materials including all those that are inert to chemical etchants and can contribute to the development of novel photonic devices and to important advances in the field of integrated photonics in the near future. Further efforts should be done in the future to reduce the propagation losses, and it represents an important challenge to improve the pedestal waveguides performance.

Authorship contributions

Julien H. Sierra: Methodology, Investigation. **Daniel O. Carvalho:** Methodoloy, Investigation. **Luciana R. P. Kassab:** Methodoloy, Conceptualization, Resources, Writing – Original Draft, Supervision, Project administration, Writing – Review & Editing, Funding acquisition. **Camila D. da S. Bordon:** Conceptualization. **Ricardo E. Samad:** Conceptualization, Methodology, Writing – Original Draft. **Niklaus U. Wetter:** Methodoloy, Conceptualization, Writing – Original Draft. **Marco I. Alayo:** Methodoloy, Conceptualization, Resources, Writing – Original Draft, Supervision, Project administration, Writing – Review & Editing, Funding acquisition.

Declaration of competing interest

The authors declare that they have no known competing financial interests or personal relationships that could have appeared to influence the work reported in this paper.

Acknowledgments

This work was performed in the framework of the National Institute of Photonics (INCT de Fotônica, 465.763/2014) project supported by the Conselho Nacional de Desenvolvimento Científico e Tecnológico (CNPq). We also thank the support from Coordenação de Aperfeiçoamento de Pessoal de Ensino Superior (CAPES). We acknowledge the Nanotechnology National Laboratory (LNNano), CNPEM-Campinas/Brazil, for the HR-TEM measurements and Fundação de Amparo à Pesquisa do Estado de São Paulo (FAPESP).

References

[1] D.O. Carvalho, M.I. Alayo, Pedestal anti-resonant reflecting optical waveguides, in: Proceedings of the SPIE 7940, Oxide-Based Materials and Devices II, Society of Photo-Optical Instrumentation Engineers (SPIE), 2011, pp. 794017–794021. https://doi.org/10.1117/12.875209.

[2] M.E. Camilo, L.R.P. Kassab, T.A.A. Assumpção, V.D.D. Cacho, M.I. Alayo, Fabrication and characterization of pedestal optical waveguides using TeO_2–WO_3–Bi_2O_3 thin film as core layer, Thin Solid Films 571 (2014) 225–229, https://doi.org/10.1016/j.tsf.2014.07.050.

[3] V.D. Del Cacho, D.M. da Silva, T.A.A. de Assumpção, L.R.P. Kassab, M.I. Alayo, E. G. Melo, Fabrication of Yb^{3+}/Er^{3+} codoped Bi_2O_3–WO_3–TeO_2 pedestal type waveguide for optical amplifiers, Opt. Mater. 38 (2014) 198–203, https://doi.org/10.1016/j.optmat.2014.10.027.

[4] T.A.A. de Assumpção, M.A. Alvarado, M.I. Alayo, L.R.P. Kassab, Production and characterization of Tm^{3+}/Yb^{3+} codoped pedestal-type PbO–GeO_2 waveguides, Can. J. Phys. 92 (2014) 597–601, https://doi.org/10.1139/cjp-2013-0591.

[5] F.A. Bomfim, D.M. da Silva, L.R.P. Kassab, T.A.A. de Assumpção, V.D. Del Cacho, M.I. Alayo, Advances on the fabrication process of Er^{3+}/Yb^{3+}: GeO_2–PbO pedestal waveguides for integrated photonics, Opt. Mater. 49 (2015) 196–200, https://doi.org/10.1016/j.optmat.2015.09.010.

[6] E.G. Melo, M.I. Alayo, D.O. Carvalho, Study of the pedestal process for reducing sidewall scattering in photonic waveguides, Opt Express 9 (2017) 9755–9760, https://doi.org/10.1364/OE.25.009755.

[7] M. Yamane, Y. Asahara, Glasses for Photonics, Cambridge University Press, Cambridge, 2000, https://doi.org/10.1017/CBO9780511541308.

[8] C.B. de Araújo, L.R.P. Kassab, Chapter 5 - enhanced photoluminescence and planar waveguide of rare-earth doped germanium oxide glasses with metallic nanoparticles, in: glass Nanocomposites: synthesis, Properties, and Applications, in: B. Karmakar, K. Rademann, A.L. Stepanov (Eds.), Micro & Nano Technologies Series, Elsevier, Cambridge, MA, 2016, pp. 132–144, https://doi.org/10.1016/B978-0-323-39309-6.00005-5. Elsevier, Oxford B. Karmakar, K. Radermann, A.L. Stepanov (Eds.), Glass Nanocomposites (2016). Synthesis, Properties and Applications.

[9] R.A.H. El-Mallawany, Tellurite Glass Smart Materials Applications in Optics and beyond, Springer, New York, 2018, https://doi.org/10.1007/978-3-319-76568-6.

[10] H.T. Munasinghe, A. Winterstein-Beckmann, C. Schiele, D. Manzani, L. Wondraczek, S. Afshar V, T.M. Monro, H. Ebendorff-Heidepriem, Lead-germanate glasses and fibers: a practical alternative to tellurite for nonlinear fiber applications, Opt. Mater. Express 3 (2013) 1488–1503, https://doi.org/10.1364/OME.3.001488.

[11] K.V. Krishnaiah, J. Marques-Hueso, R. Kashyap, Broadband emission in tellurite glasses, in: V.A.G. Rivera, D. Manzani (Eds.), Technological Advances in Tellurite Glasses: Properties, Processing and Applications, Springer, Cham, 2017, pp. 155–211, https://doi.org/10.1007/978-3-319-53038-3_8.

[12] M.M. Martins, L.R.P. Kassab, D.M. da Silva, C.B. de Araújo, Tm^{3+} doped Bi_2O_3-GeO_2 glasses with silver nanoparticles for optical amplifiers in the short-wave-infrared-region, J. Alloys Compd. 772 (2019) 58–63, https://doi.org/10.1016/j.jallcom.2018.08.146.

[13] C.D.S. Bordon, E.S. Magalhaes, D.M. da Silva, L.R.P. Kassab, C.B. de Araújo, Influence of Al_2O_3 on the photoluminescence and optical gain performance of Nd^{3+} doped germanate and tellurite glasses, Opt. Mater. 109 (2020) 110342, https://doi.org/10.1016/j.optmat.2020.110342.

[14] L.P. Naranjo, C.B. de Araújo, O.L. Malta, P.A. Santa Cruz, L.R.P. Kassab, Enhancement of Pr^{3+} luminescence in PbO–GeO_2 glasses containing silver nanoparticles, Appl. Phys. Lett. 87 (2005) 241914, https://doi.org/10.1063/1.2143135.

[15] D.M. da Silva, L.R.P. Kassab, S.R. Luthi, C.B. de Araújo, A.S.L. Gomes, M.J.V. Bell, Frequency upconversion in Er^{3+} doped PbO–GeO_2 glasses containing metallic nanoparticles, Appl. Phys. Lett. 90 (2007) 81913, https://doi.org/10.1063/1.2679798.

[16] L.R.P. Kassab, F.A. Bomfim, J.R. Martinelli, N.U. Wetter, J.J. Neto, C.B. de Araújo, Energy transfer and frequency upconversion in Yb^{3+}-Er^{3+} doped PbO-GeO_2 glass containing silver nanoparticles, Appl. Phys. B Laser Opt. 94 (2009) 239–242, https://doi.org/10.1007/s00340-008-3249-2.

[17] L.R.P. Kassab, D.S. da Silva, C.B. de Araújo, Influence of metallic nanoparticles on electric-dipole and magnetic-dipole transitions of doped germanate glasses, J. Appl. Phys. 107 (2010) 113506, https://doi.org/10.1063/1.3431347.

[18] V.P.P. de Campos, L.R.P. Kassab, T.A.A. de Assumpção, D.S. da Silva, C.B. de Araújo, Infrared-to-visible upconversion emission in Er^{3+} doped TeO_2-WO_3-Bi_2O_3 glasses with silver nanoparticles, J. Appl. Phys. 112 (2012), 063519, https://doi.org/10.1063/1.4754468.

[19] M.E. Camilo, T.A.A. Assumpção, D.M. da Silva, D.S. da Silva, L.R.P. Kassab, C.B. de Araújo, Influence of silver nanoparticles on the infrared-to-visible frequency upconversion in $Tm^{3+}/Er^{3+}/Yb^{3+}$ doped GeO_2-PbO glass, J. Appl. Phys. 113 (2013) 153507, https://doi.org/10.1063/1.4801909.

[20] M.E. Camilo, E. de O. Silva, L.R.P. Kassab, J.A.M. Garcia, C.B. de Araújo, White light generation controlled by changing the concentration of silver nanoparticles hosted by $Ho^{3+}/Tm^{3+}/Yb^{3+}$ doped GeO_2–PbO glasses, J. Alloys Compd. 644 (2015) 155–158, https://doi.org/10.1016/j.jallcom.2015.04.108.

[21] L.R.P. Kassab, D.M. Silva, J.A.M. Garcia, D.S. da Silva, C.B. de Araújo, Silver nanoparticles enhanced photoluminescence of Nd $^{3+}$ doped germanate glasses at 1064 nm, Opt. Mater. 60 (2016) 25–29, https://doi.org/10.1016/j.optmat.2016.07.006.

[22] C.B. de Araújo, T.R. Oliveira, E.L. Falcão-Filho, D.M. Silva, L.R.P. Kassab, Nonlinear optical properties of PbO–GeO_2 films containing gold nanoparticles, J. Lumin. 133 (2013) 180–183, https://doi.org/10.1016/j.jlumin.2011.09.034.

[23] L. De Boni, E.C. Barbano, T.A.A. de Assumpção, L. Misoguti, L.R.P. Kassab, S. C. Zilio, Femtosecond third-order nonlinear spectra of lead-germanium oxide glasses containing silver nanoparticles, Opt Express 20 (2012) 6844–6850, https://doi.org/10.1364/OE.20.006844.

[24] T.R. Oliveira, E.L. Falcão-Filho, C.B. de Araújo, D.S. da Silva, L.R.P. Kassab, Nonlinear optical properties of Bi_2O_3-GeO_2 glass at 800 and 532 nm, J. Appl. Phys. 114 (2013), 073503, https://doi.org/10.1063/1.4818502.

[25] J.M.P. Almeida, D.S. da Silva, L.R.P. Kassab, S.C. Zilio, C.R. Mendonça, L. De Boni, Ultrafast third-order optical nonlinearities of heavy metal oxide glasses containing gold nanoparticles, Opt. Mater. 36 (2014) 829–832, https://doi.org/10.1016/j.optmat.2013.12.012.

[26] R. Miedzinski, I. Fuks-Janczarek, L.R.P. Kassab, F.A. Bomfim, Second and third-order nonlinear optical properties of Er^{3+}/Yb^{3+} doped PbO-GeO_2-Ga_2O_3 glasses with Au nanoparticles, Mater. Res. Bull. 95 (2017) 339–348, https://doi.org/10.1016/j.materresbull.2017.08.009.

[27] E.J. Lunt, B.S. Phillips, J.M. Keeley, A.R. Hawkins, P. Measor, B. Wu, H. Schmidt, Hollow ARROW waveguides on self-aligned pedestals for high-sensitivity optical sensing, in: Proceedings of the SPIE 7591, Advanced Fabrication Technologies for Micro/Nano Optics and Photonics III, 2010, p. 759109, https://doi.org/10.1117/12.841010.

[28] E.J. Lunt, B. Wu, J.M. Keeley, P. Measor, H. Schmidt, A.R. Hawkins, Hollow ARROW waveguides on self-aligned pedestals for improved geometry and transmission, IEEE Photon. Technol. Lett. 22 (2010) 1147–1149, https://doi.org/10.1109/LPT.2010.2051145.

[29] D.M. da Silva, L.R.P. Kassab, A.L. Siarkowski, C.B. de Araújo, Influence of gold nanoparticles on the 1.53 μm optical gain in Er^{3+}/Yb^{3+}: PbO-GeO_2 RIB waveguides, Opt Express 22 (2014) 16424–16430, https://doi.org/10.1364/OE.22.016424.

[30] B.S. Ahluwalia, Ø.I. Helle, O.G. Hellesø, Rib Waveguides for trapping and transporting particles, Opt Express 24 (2016) 4477–4487, https://doi.org/10.1364/OE.24.004477.

[31] M.M. Milošević, P.S. Matavulj, P.Y. Yang, A. Bagolini, G.Z. Mashanovich, Rib waveguides for mid-infrared silicon photonics, J. Opt. Soc. Am. B 26 (2009) 1760–1766, https://doi.org/10.1364/JOSAB.26.001760.

[32] S. Lindecrantz, O.G. Hellesø, Estimation of propagation losses for narrow strip and rib waveguides, IEEE Photon. Technol. Lett. 26 (2014) 1836–1839, https://doi.org/10.1109/LPT.2014.2337055.

[33] M. Kartzow, T. Le Hiep, R.Th Kersten, Losses of optical multimode strip-waveguides made by thick film technology, Opt Commun. 29 (1979) 160–163, https://doi.org/10.1016/0030-4018(79)90007-5.

[34] K. Ogusu, Optical strip waveguide: a detailed analysis including leaky modes, J. Opt. Soc. Am. 73 (1983) 353–357, https://doi.org/10.1364/JOSA.73.000353.

[35] C. Koos, L. Jacome, C. Poulton, J. Leuthold, W. Freude, Nonlinear silicon-on-insulator waveguides for all-optical signal processing, Opt Express 15 (2007) 5976–5990, https://doi.org/10.1364/OE.15.005976.

[36] W. Bogaerts, R. Baets, P. Dumon, V. Wiaux, S. Beckx, D. Taillaert, B. Luyssaert, J. Van Campenhout, P. Bienstmann, D. Van Thourhout, Nanophotonic waveguides in silicon-on-insulator fabricated with CMOS technology, J. Lightwave Technol. 23 (2005) 401–412, https://doi.org/10.1109/JLT.2004.834471.

[37] D.J. Moss, R. Morandotti, A.L. Gaeta, M. Lipson, New CMOS-compatible platforms based on silicon nitride and Hydex for nonlinear optics, Nat. Photonics 7 (2013) 597–607, https://doi.org/10.1038/nphoton.2013.183.

[38] M. Mitchell, D.P. Lake, P.E. Barclay, Optomechanically amplified wavelength conversion in diamond microcavities, Optica 6 (2019) 832–838, https://doi.org/10.1364/OPTICA.6.000832.

[39] Z. Wang, H. Liu, N. Huang, Q. Sun, J. Wen, Impact of dispersion profiles of silicon waveguides on optical parametric amplification in the femtosecond regime, Opt Express 19 (2011) 24730–24737, https://doi.org/10.1364/OE.19.024730.

[40] M.A. Foster, A.C. Turner, J.E. Sharping, B.S. Schmidt, M. Lipson, A.L. Gaeta, Broad-band optical parametric gain on a silicon photonic chip, Nature 441 (2006) 960–963, https://doi.org/10.1038/nature04932.

[41] J. Wang, Z. Han, Y. Guo, L.C. Kimerling, J. Michel, A.M. Agarwal, G. Li, L. Zhang, Robust generation of frequency combs in a microresonator with strong and narrowband loss, Photon. Res. 5 (2017) 552–556, https://doi.org/10.1364/PRJ.5.000552.

[42] T.J. Kippenberg, R. Holzwarth, S.A. Diddams, Microresonator-based optical frequency combs, Science 332 (2011) 555–559, https://doi.org/10.1126/science.1193968.

[43] X. Xue, Y. Xuan, Y. Liu, P.-H. Wang, S. Chen, J. Wang, D.E. Leaird, M. Qi, A. W. Weiner, Mode-locked dark pulse Kerr combs in normal-dispersion microresonators, Nat. Photonics 9 (2015) 594–600, https://doi.org/10.1038/nphoton.2015.137.

[44] M. Belt, M.L. Davenport, J.E. Bowers, D.J. Blumenthal, Ultra-low-loss Ta_2O_5-core/SiO_2-clad planar waveguides on Si substrates, Optica 4 (2017) 532–536, https://doi.org/10.1364/OPTICA.4.000532.

[45] C. Chaneliere, J.L. Autran, R.A.B. Devine, B. Ballard, Tantalum pentoxide (Ta_2O_5) thin films for advanced dielectric applications, Mater. Sci. Eng. 22 (1998) 269–322, https://doi.org/10.1016/S0927-796X(97)00023-5.

[46] C.-Y. Tai, J.S. Wilkinson, N.M.B. Perney, M. Caterina Netti, F. Cattaneo, C. E. Finlayson, J.J. Baumberg, Determination of nonlinear refractive index in a Ta_2O_5 rib waveguide using self-phase modulation, Opt Express 12 (2004) 5110–5116, https://doi.org/10.1364/OPEX.12.005110.

[47] C.-L. Wu, C.-H. Hsieh, G.-R. Lin, W.-C. Chi, Y.-J. Chiu, Y.-Y. Lin, Y.-J. Hung, M.-H. Shih, A.-K. Chu, C.-K. Lee, Tens of GHz Tantalum pentoxide-based micro-ring all-optical modulator for Si photonics, Ann. Phys. 529 (2016) 1600358, https://doi.org/10.1002/andp.201600358.

[48] R.W. Boyd, Nonlinear Optics, third ed., Academic Press, 2008.

[49] G. Agrawal, Nonlinear Fiber Optics, fifth ed., Academic Press, 2012.

[50] H. El Dirani, L. Youssef, C. Petit-Etienne, S. Kerdiles, P. Grosse, C. Monat, E. Pargon, C. Sciancalepore, Ultralow-loss tightly confining Si_3N_4 waveguides and high-Q microresonators, Opt Express 27 (2019) 30726–30740, https://doi.org/10.1364/OE.27.030726.

[51] X. Ji, A.B. Felippe, S.P. Roberts, A. Dutt, J. Cardenas, Y. Okawachi, A. Bryant, A. L. Gaeta, M. Lipson, Ultra-low-loss on-chip resonators with sub-milliwatt parametric oscillation threshold, Optica 4 (2017) 619–624, https://doi.org/10.1364/OPTICA.4.000619.

[52] D.O. Carvalho, L.R.P. Kassab, V.D. Del Cacho, D.M. da Silva, M.I. Alayo, A review on pedestal waveguides for low loss optical guiding, optical amplifiers and nonlinear optics applications, J. Lumin. 203 (2018) 135–144, https://doi.org/10.1016/j.jlumin.2018.06.037.

[53] T.A.A. de Assumpção, M.E. Camilo, M.I. Alayo, D.M. da Silva, L.R.P. Kassab, Influence of gold nanoparticles on the 805 nm gain in Tm^{3+}/Yb^{3+} codoped PbO-GeO_2 pedestal waveguides, Opt. Mater. 72 (2017) 518–523, https://doi.org/10.1016/j.optmat.2017.06.031.

[54] Y. Okawachi, M.R.E. Lamont, K. Luke, D.O. Carvalho, M. Yu, M. Lipson, A.L. Gaeta, Bandwidth shaping of microresonator-based frequency combs via dispersion engineering, Opt. Lett. 39 (2014) 3535–3538, https://doi.org/10.1364/OL.39.003535.

[55] N.U. Wetter, D.S. da Silva, L.R.P. Kassab, E. Jimenez-Villar, Improving performance in ytterbium-erbium doped waveguide amplifiers through scattering by large silicon nanostructures, J. Alloys Compd. 794 (2019) 120–126, https://doi.org/10.1016/j.jallcom.2019.04.141.

[56] F.A. Bomfim, R.C. Rangel, D.M. da Silva, D.O. Carvalho, E.G. Melo, M.I. Alayo, L.R. P. Kassab, A new fabrication process of pedestal waveguides based on metal dielectric composites of Yb^{3+}/Er^{3+} codoped PbO-GeO_2 thin films with gold nanoparticles, Opt. Mater. 86 (2018) 433–440, https://doi.org/10.1016/j.optmat.2018.10.044.

[57] J.H. Sierra, R.C. Rangel, R.E. Samad, N.D. Vieira Jr., M.I. Alayo, D.O. Carvalho, Low-loss pedestal Ta_2O_5 nonlinear optical waveguides, Opt Express 27 (2019) 37516–37521, https://doi.org/10.1364/OE.27.037516.

[58] J.H. Sierra, D.O. Carvalho, R.E. Samad, R.C. Rangel, M.I. Alayo, Analysis and measurement of the non-linear refractive index of SiO_xN_y using pedestal waveguides, in: 34th Symposium on Microelectronics Technology and Devices, 2019, https://doi.org/10.1109/SBMicro.2019.8919392.

[59] D.S. Da Silva, N.U. Wetter, L.R.P. Kassab, W. De Rossi, M.S. De Araujo, Double line waveguide amplifiers written by femtosecond laser irradiation in rare-earth doped germanate glasses, J. Lumin. 217 (2020) 116789, https://doi.org/10.1016/j.jlumin.2019.116789.

[60] G.A. Al-Jumaily, S.M. Edlou, Optical properties of tantalum pentoxide coatings deposited using ion beam processes, Thin Solid Films 209 (1992) 223–229, https://doi.org/10.1016/0040-6090(92)90679-6.

[61] Y. Zhao, Y. Wang, H. Gong, J. Shao, Z. Fan, Annealing effects on structure and laser-induced damage threshold of Ta_2O_5/SiO_2 dielectric mirrors, Appl. Surf. Sci. 210 (2003) 353–358, https://doi.org/10.1016/S0169-4332(03)00153-3.

[62] J.R. Sites, P. Gilstrap, R. Rujkorakarn, Ion beam sputter deposition of optical coatings, Opt. Eng. 22 (1983) 224447, https://doi.org/10.1117/12.7973141.

[63] M.I. Alayo, I. Pereyra, W.L. Scopel, M.C.A. Fantini, On the nitrogen and oxygen incorporation in plasma-enhanced chemical vapor deposition (PECVD) SiO_xN_y films, Thin Solid Films 402 (2002) 154–161, https://doi.org/10.1016/S0040-6090(01)01685-6.

[64] M.I. Alayo, D. Criado, L.C.D. Gonçalves, I. Pereyra, Deposition and characterization of silicon oxynitride for integrated optical applications, J. Non-Cryst. Solids 338–340 (2004) 76–80, https://doi.org/10.1016/j.jnoncrysol.2004.02.025.

[65] W.L. Scopel, M.C.A. Fantini, M.I. Alayo, I. Pereyra, Local structure and bonds of amorphous silicon oxynitride thin films, Thin Solid Films 413 (2002) 59–64, https://doi.org/10.1016/S0040-6090(02)00346-2.

[66] D. Criado, I. Pereyra, M.I. Alayo, Study of nitrogen-rich silicon oxynitride films obtained by PECVD, Mater. Char. 50 (2003) 167–171, https://doi.org/10.1016/S1044-5803(03)00075-5.

[67] D. Criado, M.I. Alayo, I. Pereyra, M.C.A. Fantini, Structural analysis of silicon oxynitride films deposited by PECVD, Mater. Sci. Eng., B 112 (2004) 123–127, https://doi.org/10.1016/j.mseb.2004.05.017.

[68] D. Criado, M.I. Alayo, M.C.A. Fantini, I. Pereyra, Study of the mechanical and structural properties of silicon oxynitride films for optical applications, J. Non-Cryst. Solids 352 (2006) 2319–2323, https://doi.org/10.1016/j.jnoncrysol.2006.03.012.

[69] S.P. Zimin, E.S. Gorlachev, I.I. Amirov, H. Zogg, Micromasking effect and nanostructure self-formation on the surface of lead chalcogenide epitaxial films on Si substrates during argon plasma treatment, J. Phys. D Appl. Phys. 42 (2009) 165205, https://doi.org/10.1088/0022-3727/42/16/165205.

[70] A.A. Krokhin Nagaraj, Long-range surface plasmons in dielectric-metal-dielectric structure with highly anisotropic substrates, Phys. Rev. B 81 (2010), 085426, https://doi.org/10.1103/PhysRevB.81.085426.

[71] Y. Okamura, S. Yoshinaka, S. Yamamoto, Measuring mode propagation losses of integrated optical waveguides: a simple method, Appl. Opt. 22 (1983) 3892–3894, https://doi.org/10.1364/AO.22.003892.

[72] Y.-Y. Lin, C.-L. Wu, W.-C. Chi, Y.-J. Chiu, Y.-J. Hung, A.-K. Chu, C.-K. Lee, Self-phase modulation in highly confined submicron Ta_2O_5 channel waveguides, Opt Express 24 (2016) 21633–21641, https://doi.org/10.1364/OE.24.021633.
[73] P. Kabaciński, T.M. Kardaś, Y. Stepanenko, C. Radzewicz, Nonlinear refractive index measurement by SPM-induced phase regression, Opt Express 27 (2019) 11018–11028, https://doi.org/10.1364/OE.27.011018.
[74] K. Vu, S. Farahani, S. Madden, 980nm pumped erbium doped tellurium oxide planar rib waveguide laser and amplifier with gain in S, C and L band, Opt Express 23 (2015) 747–755, https://doi.org/10.1364/OE.23.000747.
[75] C.J. Krückel, A. Fulop, T. Klintberg, J. Bengtsson, P.A. Andrekson, V. Torres-Company, Linear and nonlinear characterization of low-stress high-confinement silicon-rich nitride waveguides, Opt Express 23 (2015) 25827–25837, https://doi.org/10.1364/OE.23.025827.
[76] V. Dimitrov, S. Sakka, Linear and nonlinear optical properties of simple oxides, J. Appl. Phys. 79 (1996) 1741, https://doi.org/10.1063/1.360963.